Size Effects in Reinforced Concrete Flanged Shear Walls

Alireza Mortezaei[1], Ali Kheyroddin[2,*]

Abstract: *The work presented in this paper investigates the causes of size effects in structural-concrete members. It is based on the use of a finite-element model found to yield realistic predictions of structural-concrete behavior in all cases investigated to date. In fact, the previous use of this model in investigations of size effects in reinforced-concrete beams indicated that such effects reflect the dependence of load-carrying capacity on small unintended eccentricities of the applied load and/or load-induced anisotropy, rather than, as widely considered, on fracture-mechanics characteristics. The present work extends the scope of the above investigation so as to include the case of reinforced concrete flanged shear walls, the behavior of which is already established experimentally. It is found that, unlike the flanged shear walls with a height-to-length ratio larger than 2, the shear walls investigated in the present work, in contrast with the interpretation given to recently published experimental findings, are size-effect independent.*

Keywords:*Flanged shear walls; Nonlinear analysis;Finite-element; Reinforced concrete; Size effects.*

1. Introduction

The load-carrying capacity of a structural-concrete member is said to be 'size-effect' dependent when its predicted values depend on the size of the member. Size effects have been first reported for the case of reinforced-concrete (RC) beams, without transverse reinforcement (stirrups), characterized by nonflexural types of failure and widely referred to as 'shear' modes of failure [1]. It has been suggested that for such a mode of failure the causes of size effects may be explained in terms of fracture-mechanics concepts, both linear [2] and non-linear [3]. In fact, the dependence of the failure load on size effects has been attributed to the release of stored elastic energy caused by crack propagation eventually leading to 'shear' failure of an RC beam [4].

Explanations of the causes of size effects, such as the above, imply that the experimentally established load-carrying capacity is essentially independent of secondary testing-procedure effects. However, this assumption underestimates the significance of small-unintended out-of-plane actions, which invariably develop in any experiment, intended to induce plane-stress conditions in specimens. Such actions may be not only due to small unintended out-of-plane eccentricities of the in-plane loads [5] (which, admittedly, may be minimized so as to become negligible), but, also, due to non-symmetrical load-induced cracking, which is inherent in concrete owing to the heterogeneous nature of this material [6].

In fact, the dependence of size effects on out-of-plane actions due to either small unintended eccentricities of the applied load or non-symmetrical load-induced cracking has already been established by comparing analysis predictions with experimental values [7]. The structural forms analyzed were mainly geometrically similar slender RC beams with a rectangular cross-section and a wide range of sizes, both without and with stirrups, the behavior of which was already established by experimental work cited in Ref. [7]. The beams analyzed were subjected to transverse loading configurations, symmetrical with respect to the middle cross-section, similar to those applied experimentally, assuming that the out-of-plane eccentricities were non-existent and significant discrepancies between experiment and analysis were found to occur only when the structural member tested was incapable of absorbing small unintended torsional effects [5]. In addition, the nonlinear finite element (FE) model [7] adopted for the analysis was capable of describing the formation of non-symmetrical load-induced cracking even for the case of a symmetrical cross-section under a symmetrical loading configuration. It should be noted, however, that such non-symmetrical cracking could also be prevented by analyzing only one of the two symmetrical portions of the beams with respect to the longitudinal plane of

* *Corresponding author:Email:akheirodin@semnan.ac.ir, Fax: 0231-3321005*

[1] *Ph.D. Candidate, Department of Civil Engineering, Engineering Faculty, Semnan University, Semnan, Iran*

[2] *Associate Professor, Department of Civil Engineering, Engineering Faculty, Semnan University, Semnan, Iran.*

symmetry at mid-breadth.

The results of the analysis demonstrated that the presence of stirrups, specified in compliance with current codes of practice so as to prevent shear types of failure, leads to predictions independent of size effects in all cases investigated. Similarly, for the case of beams without stirrups, it was found that postulating the presence of hypothetical (but, in practice, unavoidable) out-of-plane actions yields predictions of load-carrying capacities that can explain the experimental values, irrespective of the size of the beams investigated; on the other hand, ignoring out-of plane actions for all beams without stirrups led to size-effect dependent predictions of load-carrying capacity. The above results clearly demonstrate that, for the case of slender RC beams exhibiting a 'shear' type of failure, size effects are most likely to be associated with secondary testing-procedure effects rather than fracture-mechanics related properties.

The investigation of size effects for beams has been the subject of published experimental work [8 and 9]. As for the cases of slender RC beams [3 and 4], the latter experimental work was considered to indicate that the load-carrying capacities of both the short [8] and the deep [9] RC beams are size-effect dependent, and that this dependence may be dictated by fracture-mechanics related characteristics. However, the criterion employed for identifying size effects involved the use of values of the nominal shear stress at failure, which implies a 'shear' type of failure of the beams; and yet, it is widely recognized that RC beams with small values of a_v/d, without stirrups, behave as tied arches, the failure of which cannot be realistically described by a shear-failure criterion.

Shear walls are used extensively in moderate- and high-rise buildings to resist lateral loads induced by earthquakes. The seismic performance of many buildings is, therefore, closely linked to the behavior of the reinforced concrete walls. Reinforced concrete flanged shear walls are generally recognized as efficient lateral force resisting systems for multistory buildings, due to their ability to control drift demand under service load conditions as well as their inherent ductility capacity under seismic conditions. The present work extends the above analytical investigation into the causes of size effects so as to encompass the case of RC flanged shear walls exhibiting a flexural and non-flexural mode of failure.

2. Research significant

Although the experimental data provide valuable information about the behavior of R.C. structure and observed hysteretic response, they are expensive and time-consuming and design procedures are not available to assist the engineer in designing and behavior of flanged shear walls. Using the nonlinear analysis method, it is now possible, at comparatively low cost and effort, to predict the complete response of more complex R.C. members and structures such as tall structural walls. The main objective of the present work is to establish whether the behavior of RC flanged shear walls is indeed size-effect dependent. This objective is pursued by comparing experimentally established behavior [10 and 11] with predicted values. The predictions are obtained by employing the FE model. The use of this model is deemed essential for the purposes of the present work because it yields predictions which, unlike code predictions (commonly used to date in investigations of size effects), are free of any preconceived ideas regarding the mode of failure of RC structural members. There is statistical size effect as well as fracture mechanics based size effect. For FE modeling, an analysis tool which is based on layered nonlinear finite element method (NONLACS2) and investigate nonlinear behavior of flanged shear walls was used that is described next part.

3. Nonlinear finite element program

A nonlinear finite element analysis program, NONLACS2 (NONLinear Analysis of Concrete and Steel Structures), developed by Kheyroddin [12], is used to analyze the selected R.C. shear walls. The program employs a layered finite element approach and can be used to predict the nonlinear behavior of any plain, reinforced or

prestressed concrete, steel, or composite concrete-steel structure that is composed of thin plate members with plane stress conditions. This includes beams, slabs (plates), shells, folded plates, box girders, shear walls, or any combination of these structural elements. Time-dependent effects such as creep and shrinkage can also be considered.

3.1 Concrete properties

The concrete behaves differently under different types and combinations of stress conditions due to the progressive microcracking at the interface between the mortar and the aggregates (transition zone). The propagation of these cracks under the applied loads contributes to the nonlinear behavior of the concrete. As shown in Fig.1(a), the uniaxial stress-strain curve of concrete adopted in this study, is made of two parts. The ascending branch up to the peak compressive strength is represented by the equation proposed by Ashour and Morley [13]:

$$\sigma = \frac{E_0 \varepsilon}{1 + \left(\frac{E_0}{E_{sc}} - 2\right)\left(\frac{\varepsilon}{\varepsilon_{max}}\right) + \left(\frac{\varepsilon}{\varepsilon_{max}}\right)^2} \quad (1)$$

Where E_0 is the initial modulus of elasticity of the concrete, E_{sc} is the secant modulus of the concrete at the peak stress, σ is stress, ε is strain and ε_{max} is the strain at peak stress. The descending or the strain-softening branch is idealized by the Bazant et al. model [14]:

$$\sigma = \sigma_c \left(\frac{\varepsilon}{\varepsilon_{max}}\right) \exp\left(1 - \varepsilon / \varepsilon_{max}\right) \quad (2)$$

where σ_c is compressive strength of the concrete. For uniaxially loaded concrete, σ_c is equal to f'_c.

For analysis of most plane stress problems, concrete is assumed to behave as a stress-induced orthotropic material. In this study the orthotropic constitutive relationship developed by Bazant et al. model [14] is used for modeling the concrete using the smeared cracking idealization. The constitutive matrix, D, is given by:

$$D = \frac{1}{(1-\nu^2)} \begin{bmatrix} E_1 & \nu\sqrt{E_1 E_2} & 0 \\ \nu\sqrt{E_1 E_2} & E_2 & 0 \\ 0 & 0 & \frac{1}{4}(E_1 + E_2 - 2\nu\sqrt{E_1 E_2}) \end{bmatrix} \quad (3)$$

in which, E_1 and E_2 are the tangent moduli in the directions of the material orthotropy, and is the Poisson's ratio. The orthotropic material directions coincide with the principal stress directions for the uncracked concrete and these directions are parallel and normal to the cracks for the cracked concrete. The concept of the "equivalent uniaxial strain" developed by Darwin and Pecknold [15] is utilized to relate the increments of stress and strain in the principal directions. Therefore, stress-strain curves similar to the uniaxial stress-strain curves can be used to formulate the required stress-strain curves in each principal direction.

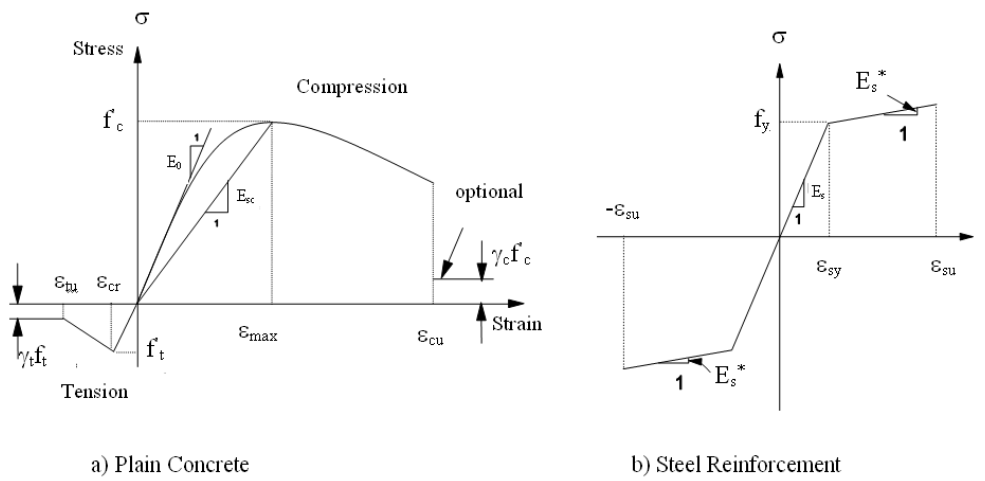

a) Plain Concrete b) Steel Reinforcement

Fig.1 Uniaxial stress-strain curves

The strength of concrete, σ_c, and the values of E_1, E_2 and v are functions of the level of stress, and the stress combinations. The concrete strength when subjected to biaxial stresses is determined using the failure envelope developed by Kupfer et al. [16]. The values of E_1 and E_2 for a given stress ratio ($\alpha = \sigma_1/\sigma_2$) are found as the slopes of the $\sigma_1-\varepsilon_1$ and $\sigma_2-\varepsilon_2$ curves, respectively. For the descending branches of both compression and tension stress-strain curves, E_i is set equal to a very small number, 0.0001, to avoid computational problems associated with a negative and zero values for E_i. The concrete is considered to be crushed, when the equivalent compressive strain in the principal directions exceeds the ultimate compressive strain of the concrete, ε_{cu}. For determination of the concrete ultimate compressive strain, ε_{cu}, two models for unconfined high and normal-strength concrete (Pastor [17]) and confined concretes (Chung et al. [18]) are implemented into the program.

For elimination of the numerical difficulties after crushing ($\varepsilon > \varepsilon_{cu}$) and cracking of the concrete ($\varepsilon > \varepsilon_{tu}$), a small amount of compressive and tensile stress as a fraction of concrete strength, $\gamma_c f'_c$ and $\gamma_t f'_t$, is assigned (optional) at a high level of stress (Fig.1(a)), where parameters γ_c and γ_t define the remaining compressive and tensile strength factors, respectively.

3.2 Crack modeling techniques

Cracking of the concrete is one of the important aspects of material nonlinear behavior of the concrete. Besides reducing the stiffness of the structure, cracks have resulted in redistribution of stresses to the reinforcing steel as well as increasing the bond stress at the steel-concrete interface [19]. Cracking of the concrete is idealized using the fixed smeared cracking model and is assumed to occur when the principal tensile stress at a point (usually a Gauss integration point) exceeds the tensile strength of the concrete. After cracking, the axes of orthotropy are aligned parallel and orthogonal to the crack. The elastic modulus perpendicular to the crack direction is reduced to a very small value close to zero and the Poisson effect is ignored. The effect of the crack is smeared within the element by modifying the [D] matrix. If σ_1 exceeds the tensile strength of concrete, f'_t, the material stiffness matrix is defined as (one crack is opened):

$$[D] = \begin{bmatrix} 0 & 0 & 0 \\ 0 & E_2 & 0 \\ 0 & 0 & \beta G \end{bmatrix} \quad \text{Where } 0 < \beta \leq 1.0 \qquad (4)$$

Once one crack is formed, the principal directions are not allowed to rotate and a second crack can form only when $\sigma_2 > f'_t$, in a direction perpendicular to the first crack. Then,

$$[D] = \begin{bmatrix} 0 & 0 & 0 \\ 0 & E_2 & 0 \\ 0 & 0 & \beta G \end{bmatrix} \quad \text{Where } 0 < \beta \leq 1.0 \qquad (5)$$

The shear retention factor, β, with a value of less than unity, serves to eliminate the numerical difficulties that arise if the shear modulus is reduced to zero, and more importantly, it accounts for the fact that cracked concrete can still transfer shear forces through aggregate interlock and dowel action. Due to the bond between the concrete and the steel reinforcement, a redistribution of the tensile stress from the concrete to the reinforcement will occur [20]. In fact, the concrete is able to resist tension between the cracks in the direction normal to the crack; this phenomenon is termed tension-stiffening. The tension-stiffening effect is idealized by assuming the ascending and the descending branches of the tensile stress-strain curve to terminate at ε_{cr} and ε_{tu}, respectively .For evaluation of an "appropriate" value of the ultimate tensile strain of the concrete, ε_{tu}, and elimination of mesh size dependency phenomenon, Shayanfar et al [21] proposed the following simple formula:

$$\varepsilon_{tu} = 0.004\ e^{-0.008\ h} \qquad (\varepsilon_{tu} \geq \varepsilon_{cr}) \qquad (6)$$

Where h is the width of the element in mm and ε_{cr} is the concrete cracking strain. For elimination of the element size effect phenomenon, both the new proposed model and

the crack band model, based on fracture mechanics, proposed by Bazant and Oh [22] have been implemented into the NONLACS2 program.

3.3 Reinforcing bar properties

The reinforcing bars are modeled as an elastic strain-hardening material as shown in Fig. 1(b). The reinforcing bars can be modeled either as smeared layers or as individual bars. In both cases, perfect bond is assumed between the steel and the concrete.

3.4 Finite element formulation

The element library includes plane membrane, plate bending, one dimensional bar, shear connecter, spring boundary elements as well as a facet shell element, which is a combination of the plane membrane and the plate bending elements. Figure 2 shows some of these elements and the associated degrees of freedom. The two nodes, three degrees of freedom per node one dimensional bar element is used to model uniaxial truss members, unbonded prestressed tendons and shear connectors. The program employs a layered finite element approach. The structure is idealized as an assemblage of thin constant thickness plate elements with each element subdivided into a number of imaginary layers as shown in Fig. 2(c). A layer can be either of concrete, smeared reinforcing steel or a continuous steel plate. The number of layers depends on the behavior of the structure being analyzed. Each layer is assumed to be in a state of plane stress, and can assume any state-uncracked, partially cracked, fully cracked, non-yielded, yielded and crushed -depending on the stress or strain conditions.

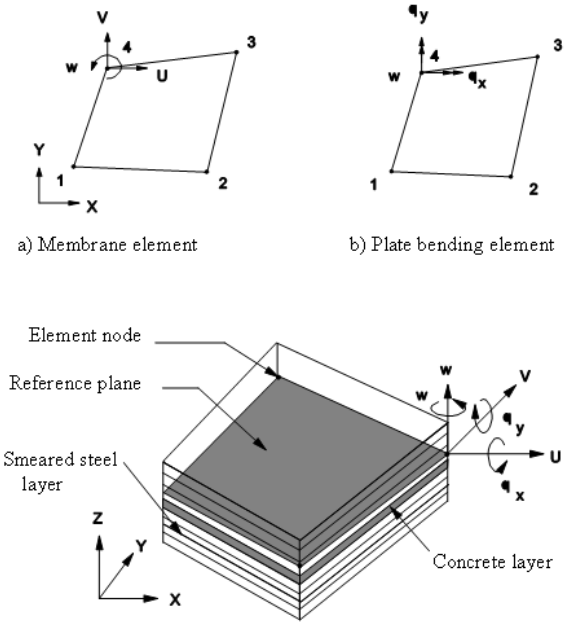

Fig.2 Some typical finite elements in NONLACS2 Program

3.5 Nonlinear analysis method

Nonlinear analysis is performed using an incremental-iterative tangent stiffness approach and the element stiffness is obtained by adding the stiffness contributions of all layers at each Gauss quadrature point. The change in the material stiffness matrix during loading necessitates an incremental solution procedure with a tangent stiffness scheme that using piece-wise linearization has been adopted in the NONLACS2 program.

4. RC flanged shear walls investigated

The RC flanged shear walls analytically investigated in the present work are shown in Fig.3. This figure was reproduced from Ref [10], where a detailed description of the experimentally established shear wall behavior is provided. The design details of the shear walls depicted in the figure are complemented with

Table 1 Design details and experimentally established failure loads of RC shear walls in Ref. [10] (f_y=510 MPa in all cases)

Specimen	Overal height (mm)	Flange width (mm)	Web length (mm)	F_c (MPa)	V_u (kN)
SW711	680	200	200	18.1	165
SW022	1030	400	400	19.9	270
SW511	1380	600	600	19.8	350
SW411	1780	800	800	19.4	365
SW211	2250	1000	1000	20	505

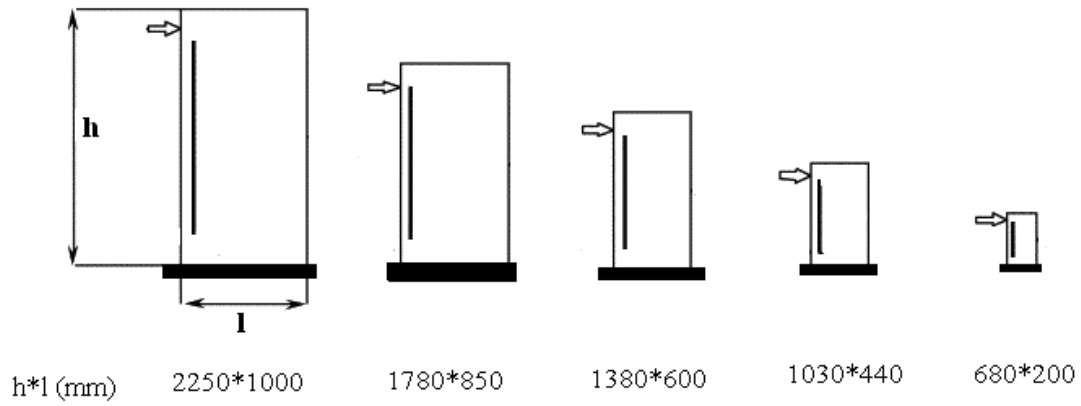

Fig.3 Schematic representation of RC shear walls in Ref. [10] (see Table 1) investigated analytically in the present work. (From left to right: SW711, SW022, SW511, SW411, SW211.)

additional information included in Table 1 and Table 2.

As indicated in the figure the shear walls were subjected to point loading. In order to prevent bearing failure, load and reaction were transmitted to the shear walls through rigid steel platens with a sufficiently large loading surface to prevent bearing stresses from exceeding critical levels. Moreover, as an additional precaution against bearing failure of the shear walls, the specimens were reinforced in the regions of the point load in a manner leading to the formation of a concealed short column.

5. Verification and Applications

The capability of NONLACS2 program to reliably simulate the fundamental behavior arising from elastic and inelastic flexure interaction was verified by correlating analytically simulated and measured response of

Table 2 Design details and experimentally established failure loads of RC shear walls in Ref. [10] (, f_y=510 MPa in all cases)

Shear wall	Height	Flange width	web length	ratio	Curing age, days	f_c MPa	V_u kN
1-500/0.50	1500	500	500	0.56	109	49.1	850
1-500/0.75	1750	500	500	0.84	108	42.5	700
1-500/1.00	2000	500	500	1.13	106	37.4	570
2-1000/0.50	2000	1000	1000	0.56	43	31.2	875
2-1000/0.75	1480	1000	1000	0.84	38	32.7	650
2-1000/1.00	3000	1000	1000	1.13	35	30.8	435
3-1400/0.50	2410	1400	1400	0.56	72	32.8	1175
3-1400/0.75	3100	1400	1400	0.84	32	36.2	950
3-1400/1.00	3840	1400	1400	1.13	66	35.3	800
4-1750/0.50	2760	1750	1750	0.56	56	42.6	1636
4-1750/0.75	3640	1750	1750	0.84	55	40.4	1240
4-1750/1.00	4520	1750	1750	1.13	47	44.8	1000

three works. In each case, different forms of output (including mode of failure) were extracted and compared with experimental results to verify key aspects of the numerical model. Although some discrepancies were observed, the overall match between the analytical models and experimental tests was good.

5.1. Kwak and Kim RC shear panels

The experimental results from reinforced concrete shear panels tested by Kwak and Kim [23] are widely used to validate the analytical models for reinforced concrete membrane element. These panels were orthogonally reinforced, and had identical dimensions of 890 mm×890 mm×70 mm. Lateral load was imposed on the top-right joint and the axial load was spread along the top rows of joint. Fig.4 shows the configuration of the test specimen and the finite element grid used. The finite element used in this study is an isoparametric 4-node element

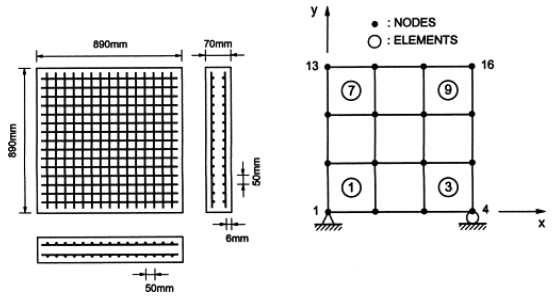

Fig.4 Configuration and finite element idealization of panels.

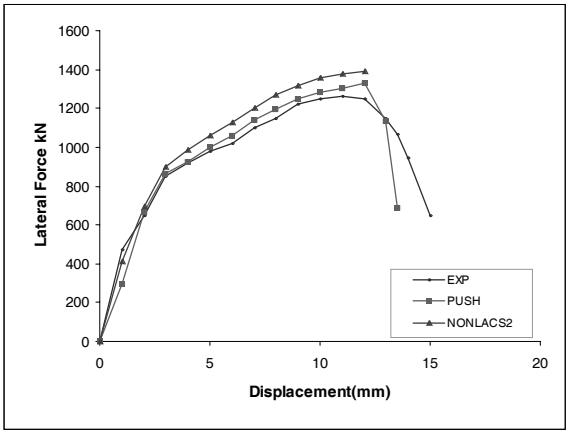

Fig.5 Comparison of experimental and analytical results of Kwak and Kim RC shear panels

with 2×2 Gauss integration because all the stresses at every Gauss point are the same values and the 4-node element gives more stable stress results through the loading history. The assumed material properties were as follows: Poisson's ratio =0.2, the tensile strength of concrete, $f_t' = 0.33\sqrt{f_c'}$ MPa, the elastic modulus of steel E_{s1}=200,000 MPa, E_{s2}=0.01 E_{s1}.

A two-dimensional static monotonic analysis was performed by Kwak and Kim [23]. For modeling of shear wall in NONLACS2 program, have been used four-node shell elements, QLC3 type as plane stress and bending. Results analyses are plotted in Fig.5 along with the envelope response of the two-dimensional pushover analysis and the experimental response of the specimen. In spite of the exact predictions in the failure modes, the analysis slightly overestimates the shear strength of the panels. In addition, the numerical results still give more exact predictions for the shear strength of a shear dominant structure because the prediction by code guidelines represents the large overestimate. Totally, the result indicated that NONLACS2 programs provide reasonable results and can be used to approximate ultimate load. An ultimate load of 1390 KN was reported for shear panel.

5.2 Wallace and Thomsen flanged walls (1995)

Wallace and Thomsen [24] conducted tests of T-shaped RC walls subjected to axial compression and cyclic lateral loading. Using measured material properties and dimensions, the

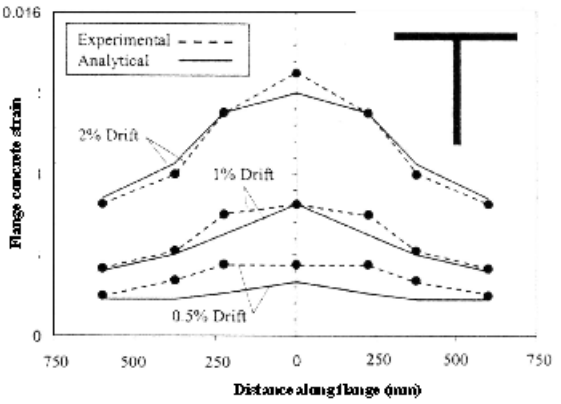

Fig.6 Measured and computed tension flange strain profile for Specimen TW2 [24]

monotonic and cyclic responses of Wall TW2 are calculated and compared with the test results. The measured and calculated load-deflection curves match well. As shown in Fig.6, the measured strain distribution in the flange under tension also compares well to the computed strains for various drift levels. Because the model cannot capture local bar buckling, it was unable to predict the initiation of these modes of failure as observed in the tests. Nevertheless, the analytical results correlate well to the test data prior to the occurrence of these local modes of failure.

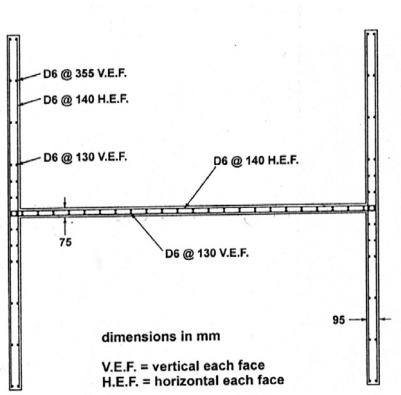

Fig.8 Top view of wall reinforcement [11]

5.3 Vecchio and Palermo flanged walls (2002)

Five large-scale flanged shear walls tested under static cyclic displacement by Palermo and Vecchio (2002) [11]. The specimens were constructed with stiff top and bottom slabs. The top slabs (2600?1440?150 mm) served to distribute the horizontal and axial load to the walls of the structure. The bottom slab (2600?1440?300 mm), clamped to the laboratory strong floor, simulated a rigid foundation. The slabs were reinforced with NO.30 (29.9 mm) deformed reinforcing bars at a spacing of 350 mm in each direction, with a top and bottom layer.

The web wall was reinforced with D6 reinforcing bars, the bars were spaced 140 mm horizontally and 130 mm vertically in two parallel layers. The flange walls were approximately 95 mm thick. The flanges were also reinforced with D6 reinforcing bars, spaced 140 mm horizontally and 130 mm vertically near the web wall and 255 mm near the tips of the flanges. The concrete clear covers in the walls and slabs were 15 and 50 mm, respectively. Dimensional details of the walls are shown in Fig.7 and the reinforcement layout for the web and flange walls are given in Fig.8. Details of the concrete and reinforcement properties are given in Table 2.

The RC flanged shear wall shown in Fig.7 and Fig.8 were modeled as indicated in Fig.10, which shows typical FE meshes adopted for the dicretization of the shear walls. It is important to note that for all shear walls investigated, the FE meshes comprised finite elements with a similar size. In fact, the deviation of any element size from the mean value of all element sizes used for the discretization of the shear walls did not exceed 30% of the mean value. As explained in Ref. [21], the FE model's results are independent of the FE size, but no element in the mesh is ever made smaller than about 3 times the aggregate size of the mix since the assumption of homogeneity would break down and, also, there is simply no material data for elements much

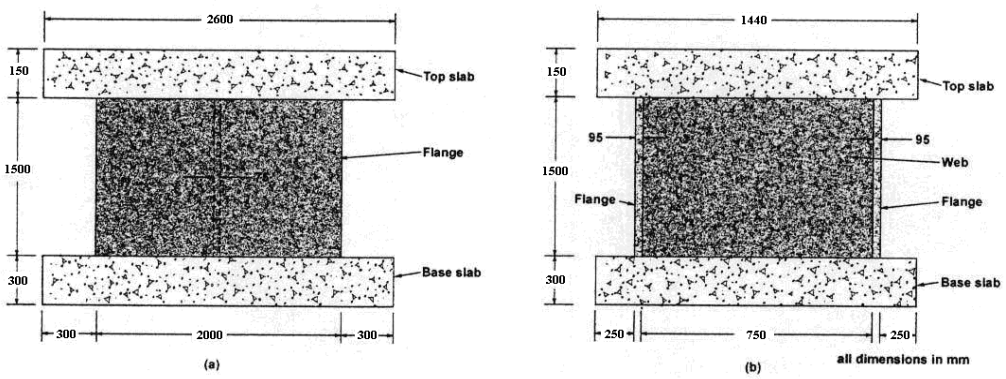

Fig.7 Test specimen details: (a) end view; (b) side view. [11]

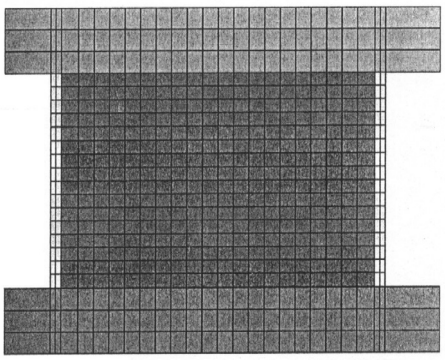

Fig.9 Finite element mesh configuration

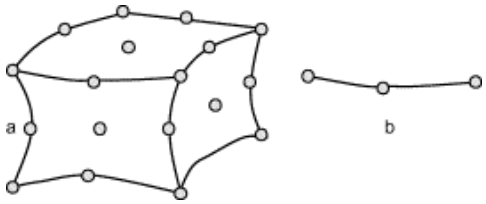

Fig.10 Finite elements used for modeling (a) concrete and (b) steel

smaller than the cube or cylinder specimens used to obtain such material properties. For clarity purposes, the figures do not indicate the location of the line elements used to model the longitudinal and transverse reinforcement. Such elements modeling the main longitudinal bars formed three lines coinciding with the lines connecting the three rows of brick-element nodes at the bottom face of the shear wall models. On the other hand, the web reinforcement was uniformly distributed along the boundaries of the brick elements in the longitudinal and transverse directions on the side, top and bottom faces of the shear wall models.

The finite element mesh, shown in Fig.9, consisted of 540 constant strain rectangular elements. The mesh was divided into four zones: the web wall, flange walls, top slabs, and bottom slabs. For modeling of I-shaped shear wall in NONLACS2 program, have been used 27-node Lagrangian brick element, QLC3 type that is used for modeling concrete, while element LM03 is a 3-node parabolic element, with axial stiffness only (on account of the negligible role of dowel action [20]), used for modeling the reinforcing bars (Fig.10). The main feature of the model is its heavy dependence on a careful and realistic description of the concrete behavior (especially its triaxial response as cracking propagates), which sharply contrasts with those adopted by other FE structural-concrete models.

The shear wall specimens were subjected to the combined action of the uniformly distributed axial load and the horizontal load which was monotonically increased to failure. It is also important to note that, in order to prevent failure in the region of applied point loads or reactions, such regions were modeled by a single concrete element which was not allowed to fail throughout the loading history of the shear walls. In fact, in order to safeguard against such a type of failure, the shear walls tested in the work described in Ref. [11] were locally over-reinforced.

6. Results of analysis

The main results of the analysis are summarized in Table 3 and Table 4 and Fig.11, Fig.12, Fig.13, Fig.14, Fig.15 and Fig.16. Table 3 and Table 4 include the values of the load-carrying capacity predicted by the analysis together with those established experimentally for the shear walls shown in Fig.3. In the tables, the load-carrying capacity is expressed both in the form of the maximum shear force sustained by the shear walls and in a normalized form usually adopted in investigations of size effects. Fig.11 provides a graphical representation of the correlation of the values of the load-carrying capacity predicted by analysis with those established experimentally, while Fig.12 presents the analytical and experimental load-deflection curves of the shear walls shown in Fig.1. Fig.13 provides a graphical representation of the correlation between the analytical values of the load-carrying capacity of all shear walls investigated, normalized with respect to their experimental counterparts, and the size of the shear walls expressed in terms of the shear wall length. Similar correlations for each of the av/d values investigated are shown in Fig.14(a)–(c),

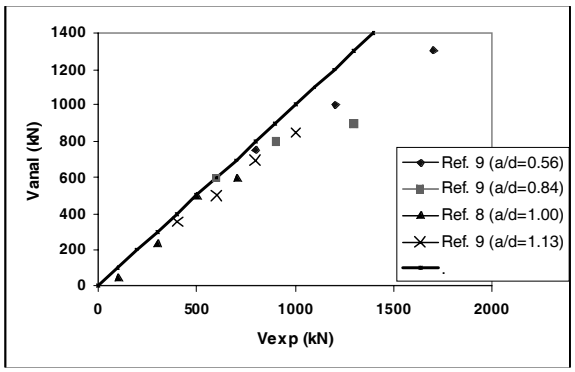

Fig.11 Graphical correlation between predicted and experimental values of load-carrying capacity.

where the analytical and experimental values are presented separately, expressed in a normalized form. Finally, Fig.15 shows typical crack patterns predicted by the analysis at the maximum sustained load together with the corresponding experimentally established modes of failure in Fig.16.

7. Discussion of results

The analytical results included in Table 3 and Table 4 and depicted in Fig.11 and Fig.12 reaffirm the ability of the FE model employed in the present work to yield realistic predictions of

Table 3 Analytical and experimental values of load-carrying capacity of RC shear walls in Ref. [8]

Specimen	V_{ANAL} (kN)	$v_{ANAL}=V_{ANAL}/f_c bd$	V_{EXP}(kN)	$v_{EXP}=V_{EXP}/f_c bd$	V_{EXP}/V_{ANAL}
SW711	120	0.166	165	0.228	1.37
SW022	252	0.141	270	0.151	1.07
SW511	360	0.13	350	0.126	0.97
SW411	360	0.1	365	0.102	1.02
SW211	480	0.103	505	0.109	1.06

Table 4 Analytical and experimental values of load-carrying capacity of RC shear walls in Ref. [9]

Specimen	V_{ANAL} (kN)	$v_{ANAL}=V_{ANAL}/f_c bd$	V_{EXP} (kN)	$v_{EXP}=V_{EXP}/f_c bd$	V_{EXP}/V_{ANAL}
1-500/0.5	648	0.212	850	0.278	1.311
2-1000/0.5	780	0.202	875	0.226	1.12
3-1400/0.5	1014	0.177	1175	0.204	1.15
4-1750/0.5	1296	0.139	1636	0.176	1.26
1-500/0.75	630	0.238	700	0.265	1.11
2-1000/0.75	588	0.145	650	0.161	1.11
3-1400/0.75	780	0.123	950	0.15	1.22
4-1750/0.75	936	0.106	1240	0.14	1.32
1-500/1	432	0.186	570	0.245	1.31
2-1000/1	420	0.11	435	0.114	1.03
3-1400/1	660	0.107	800	0.129	1.21
4-1750/1	840	0.086	1000	0.102	1.18

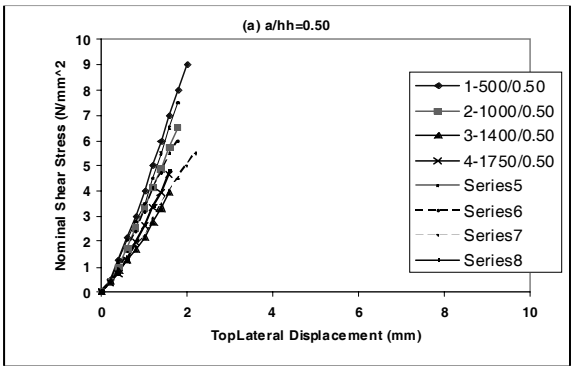

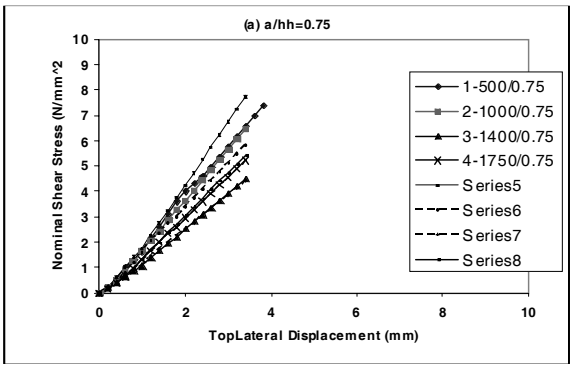

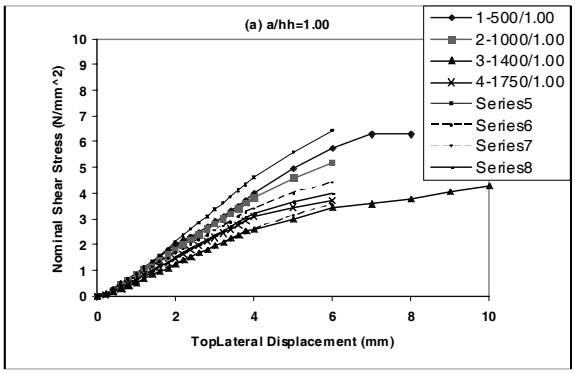

Fig.12 Predicted and measured load-deflection curves of RC shear walls (dashed lines indicating predictions).

structural-concrete behavior. Such predictions involve both the load-carrying capacity (see Table 3 and Table 4 and Fig.11) and the deformational behavior (see Fig.12) of the shear walls investigated in the present work. In fact, Fig.11 indicates that the largest deviation of the predictions from the diagonal line of the plot, which represents the ideal correlation between predicted and measured values of the load-carrying capacity, is of the order of 30%, with most predictions exhibiting a significantly smaller deviation from the diagonal. On the other hand, as regards the deformational response of

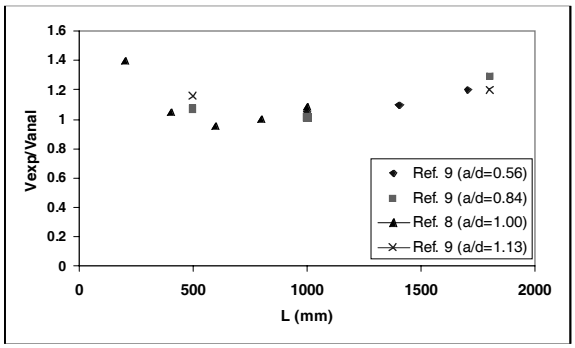

Fig.13 Graphical representation of variation with shear wall length of the predicted values of load-carrying capacity normalized with respect to their experimental counterparts

the shear walls analyzed, Fig.12 indicates a close correlation between predicted and experimentally established load-deflection curves, with the correlation being almost perfect for the cases of a_v/d=0.56 and a_v/d=1.13.

The use of the present FE model for the investigation of the causes of size effects in shear walls with an a_v/d larger than 2 established that such effects reflect the development of small unintended out-of-plane eccentricities, predominantly caused by load-induced non-symmetrical cracking. In contrast with the above findings, Fig.13 indicates that, for the cases of shear walls with an a_v/d smaller than 2, load-carrying capacity is essentially independent of size effects since the FE model predictions and the test data show good correlation independently of beam size. The dependence of the behavior of a structural-concrete member on size effects is usually manifested by predicted values of load-carrying capacity which overestimate their experimental counterparts in a manner that the deviation of the former from the latter values increases with the size of the members. And yet, none of the above characteristics is exhibited by the trends of behavior depicted in Fig.13. In fact, quite the opposite is found to be the case, i.e. the experimental values of load-carrying capacity are consistently larger than the predicted ones. Moreover, while the difference between the two sets of values is essentially independent of the member size, the larger discrepancies occur mainly in the case of the smaller shear walls which is incompatible with the trend associated with "size effects".

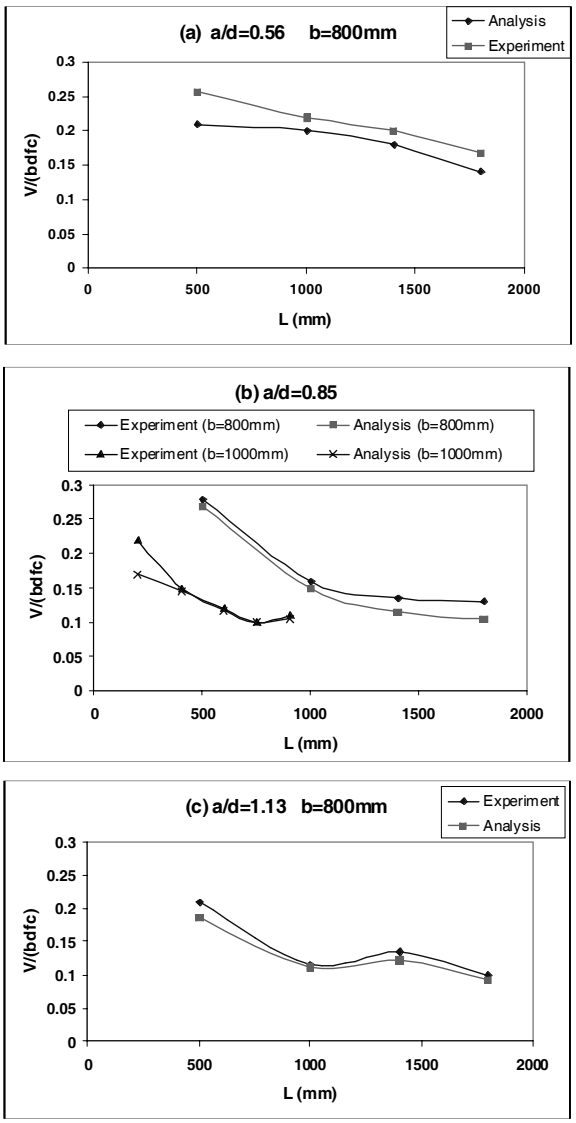

Fig.14 Graphical representation of variation with shear wall length of the predicted and measured values of load-carrying capacity expressed in the form of nominal shear stress normalized with respect to the cylinder compressive stress f_c.

The above difference in behavior regarding "size effects" exhibited between shear walls with a_v/d 2 and shear walls with a_v/d>2 reflects the wider differences in behavior characterizing RC shear walls with such values of a_v/d [25]. As described in Ref. [25], the causes of failure of RC shear walls are associated with the development of tensile stresses normal to the compressive stress trajectories. For shear walls with a_v/d>2, such stresses develop within the compressive zone, which, due to its small volume, does not

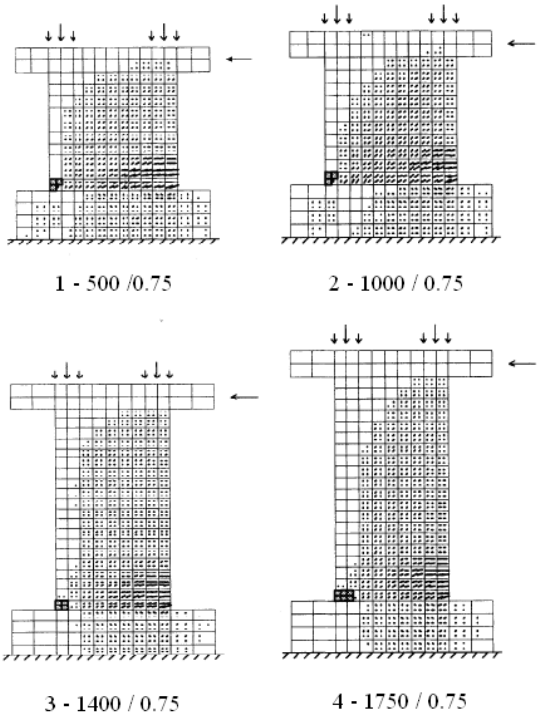

Fig.15 Typical predicted crack patterns at maximum sustained load together with the corresponding experimentally established modes of failure for shear walls 1-500/0.75, 2-1000/0.75, 3-1400/0.75 and 4-1750/0.75.

have the capacity to absorb—through redistribution—the effect of any additional such stresses caused by out-of-plane actions. As a result, the shear wall's load-carrying capacity is very sensitive to the development of the above additional stresses, which eventually lead to "premature" failure. On the other hand, for shear walls with the values of a_v/d investigated in the present work, the tensile stresses develop within the shear wall web. The shear wall web, in contrast with the compressive zone, is sufficiently large to provide the space required for the redistribution of any additional tensile stresses due to out-of-plane action in a manner that their effect on load-carrying capacity is negligible.

On the other hand, it is interesting to note in Fig.14 that expressing the load-carrying capacity in the form of a nominal shear stress yields a variation with the shear wall length which, for both the analytical and the experimental values,

Fig.16. Experimentally established failure mode of a typical shear wall (shear wall 4-1750/1.00).

exhibits the trend widely considered to be indicative of size-effect dependency. For the case of the experimentally established load-carrying capacity, to consider the above trend as indicative of size-effect dependency implies that the concept of "shear capacity of a critical section" provides a suitable failure criterion for the shear walls investigated in the present work. This is an essentially elastic or "allowable stress" concept, where failure is assumed to occur when the average applied shear stress (obtained from the ratio of applied shear force to the cross-sectional area bd) exceeds a critical value. However, this criterion is not valid for shear walls with a value of a_v/d smaller than approximately 2, in which "shear" failure occurs as a consequence of interacting flexure and shear. The present analysis, on the other hand, uses the true (triaxial) failure criterion for concrete and analyses the shear wall as a whole: the results show that the predictions are close to the experimental data and hence there are no size effects.

Fig.15 shows typical predictions of the crack patterns at the load step preceding that causing collapse of three of the shear walls (2-1000/0.75, 3-1400/0/75 and 4-1750/0.75) investigated. The figure also includes the corresponding modes of failure of the shear walls established by experiment. It is interesting to note in the figure that inclined cracking penetrated deeper into the compressive zone than flexural cracking, and this, which occurred for all shear walls investigated, is in agreement with the

experimental observations. As the smeared-crack approach adopted for modeling the cracking process is by itself unable to predict crack widths, the position of the wider cracks forming in a shear wall has been identified by the location (indicated by the thick dots in the figure) of the largest strains developing in the steel bar crossing a crack. In fact, the figure indicates that the above crack predictions are in close agreement with the experimentally observed main crack patterns associated with the relevant mode of failure.

8. Conclusions

The present work reaffirms the ability of the FE model used for the analysis to yield close predictions of structural-concrete behavior. Unlike shear walls with $a_v/d>2$, for which the use of the above model indicated that the causes of size effects are dictated by out-of-plane actions predominantly related with load-induced anisotropy, shear walls with $a_v/d<2$ are found to be independent of size effects. In fact, the form of representation considered in the literature as indicative of such effects is meaningless, as it does not provide a unique relationship between shear wall behavior and shear wall size.

References

[1] G.N.J. Kani. How safe are our large reinforced concrete beams. ACI J. 64 3 (1967), pp. 128–141.

[2] Reinhardt HW. Similitude of brittle fracture of structural concrete. In: Advanced Mechanics of Reinforced Concrete, IABSE Colloquium, 1988. p. 175–84

[3] Z.P. Bazant and J.K. Kim, Size effect in shear failure of longitudinally reinforced beams. ACI J. 81 5 (1984), pp. 456–468. Also Discussion in Z.P. Bazant and J.K. Kim. ACI J. 82 4 (1985), pp. 579–583.

[4] Z.P. Bazant and M.T. Kazemi, Size effect on diagonal shear of beams without stirrups. ACI Struct. J. 88 3 (1991), pp. 268–274.

[5] M. D. Kotsovos and M.N. Pavlovi , A possible explanation for size effects in structural concrete. Arch. Civ. Eng. (Pol. Acad. Sci.) 40 2 (1994), pp. 243–261.

[6] M.D. Kotsovos and M.N. Pavlovi , Size effects in structural concrete: a numerical experiment. Comput. Struct. 64 (1997), pp. 285–295.

[7] M. D. Kotsovos and M.N. Pavlovi , Structural concrete: finite-element analysis for limit-state design. , Thomas Telford, London (1995).

[8] J. Walraven and N. Lehwalter, Size effects in short beams loaded in shear. ACI Struct. J. 91 5 (1994), pp. 585–593.

[9] K.H. Tan and H.Y. Lu, Shear behavior of large RC deep beams and code comparisons. ACI Struct. J. 96 5 (1999), pp. 836–845.

[10] Vecchio F.J., (1999). Towards Cyclic Load Modeling of Reinforced Concrete, ACI Structural Journal, Vol. 96, No.2, March-April, pp. 389-407.

[11] Vecchio F.J. and Palermo D., (2002). Behavior of Three Dimensional Reinforced Concrete Shear Walls", ACI Structural Journal, Vol. 99, No. 1, January.

[12] Kheyroddin, A. (1996). "Nonlinear Finite Element Analysis of Flexure-Dominant Reinforced Concrete Structures", Ph.D. Thesis, Department of Civil Engineering and Applied Mechanics, McGill University, Montreal, Canada, 290p.

[13] Ashour A. F. and Morley C. T. (1993). Three-dimensional nonlinear finite element modelling of reinforced concrete structures, Finite Elements in Analysis and Design, Vol. 15, Issue 1, December, pp. 43-55.

[14] Bazant Z.P., Belytschko T., Yul-Woong H. and Ta-Peng C., (1986). Strain-softening

materials and finite-element solutions, Computers & Structures, Vol. 23, Issue2, pp. 163-180.

[15] Darwin, D. and Pecknold D.A. (1977). Nonlinear Biaxial Stress-Strain Law for Concrete, ASCE Journal of the Engineering Mechanics Division, Vol. 103, No. EM4, pp. 229-241.

[16] Kupfer, H. B., Gerstle, K. H. and Rusch, H. (1969). Behavior of Concrete Under Biaxial Stresses ACI Strucutural Journal, Vol. 66, No. 8, pp. 656-666.

[17] Pastor, J.A. (1986). High-Strength Concrete Beams, Ph.D. Thesis, Cornell University, New York, Ithaca.

[18] Chung H., Yang K., Lee Y. and Eun H. (2002). Stress–strain curve of laterally confined concrete, Engineering Structures, Vol. 24, Issue 9, September, pp. 1153-1163.

[19] Sundara Raja Iyengar K.T., Raviraj S. and Jayaram T.N. (2002). Analysis of crack propagation in strain-softening beams, Engineering Fracture Mechanics, Vol. 69, Issue 6, April, pp. 761-778.

[20] Martín-Pérez B. and Pantazopoulou S.J. (2001). Effect of bond, aggregate interlock and dowel action on the shear strength degradation of reinforced concrete, Engineering Structures, Vol. 23, Issue 2, February, pp. 214-227.

[21] Shayanfar, M.A., Kheyroddin, A. and Mirza, M.S. (1997). Element Size Effects in Nonlinear Analysis of R.C. Members, Computer & Structure, Vol.62, No.2, PP. 339-352.

[22] Bazant, Z. P. and Oh, B.H. (1983). Crack Band Theory for Fracture of Concrete, Material and Structures, Vol. 16, No. 93, pp. 155-177.

[23] Kwak H. and Kim D., (2006). Cracking behavior of RC panels subject to biaxial tensile stresses, Computers & Structures, Vol. 84, Issues 5-6, January, pp. 305-317.

[24] Wallace, J.W., Thomsen, J.H. (1995). Seismic Design of RC Structural Walls", ASCE Journal of Structural Engineering, Vol.121, No.1, January, pp. 88-101.

[25] Wang T. and Hsu T.T. Nonlinear finite element analysis of concrete structures using new constitutive models, Computers & Structures, Volume 79, Issue 32, December 2001, Pages 2781-2791